Infrared optical properties of the spin-$\frac{1}{2}$ quantum magnet TiOCl

G. Caimi
Laboratorium für Festkörperphysik, ETH Zürich, CH-8093 Zürich, Switzerland

L. Degiorgi
Paul Scherrer Institute, CH-5232 Villigen and Laboratorium für Festkörperphysik, ETH Zürich, CH-8093 Zürich, Switzerland

N. N. Kovaleva and P. Lemmens
Max Planck Institute for Solid State Research, Heisenbergstrasse 1, D-70569 Stuttgart, Germany

F. C. Chou
Center for Materials Science and Engineering, Massachusetts Institute of Technology, Cambridge, Massachusetts 02139, USA
(Received 12 August 2003; revised manuscript received 6 November 2003; published 22 March 2004)

We report results on the electrodynamic response of TiOCl, a low-dimensional spin-$\frac{1}{2}$ quantum magnet that shows a spin gap formation for $T<T_{c1}=67$ K. The Fano-like shape of a few selected infrared active phonons suggests an interaction between lattice vibrations and a continuum of low-frequency (spin) excitations. The temperature dependence of the phonon mode parameters extends over a broad temperature range well above T_{c1}, indicating the presence of an extended fluctuation regime. In the temperature interval between 200 K and T_{c1}, there is a progressive dimensionality crossover (from two to one), as well as a spectral weight shift from low towards high frequencies. This allows us to identify a characteristic energy scale of about 430 K, ascribed to a pseudo-spin-gap.

DOI: 10.1103/PhysRevB.69.125108 PACS number(s): 78.20.−e, 71.36.+c

I. INTRODUCTION

Low-dimensional quantum spin systems, based on complex transition-metal oxides, have recently attracted a lot of attention, particularly as a fascinating playground to study spin-charge separation, spin-gap states, and quantum disorder. Proposals that the exotic properties of low-dimensional spin-$\frac{1}{2}$ quantum magnets might also play a major role in shaping the mechanism for high-temperature superconductivity led to vigorous experimental activity on materials involving Cu^{2+} ions with a $3d^9$ configuration ($S=\frac{1}{2}$). Other examples of $S=\frac{1}{2}$ are notably Ti^{3+} and V^{4+} systems in d^1 configuration (i.e., one single d electron occupies one of the t_{2g} orbitals). In this respect, the layered Ti$O$$X$ (X=Cl and Br) compounds are most promising and are candidates for exotic electronic configurations, as in the resonating-valence-bond (RVB) model[1] and for superconductivity based on dimer fluctuations.[2,3]

TiOCl was first considered as a two-dimensional antiferromagnet, an electron analog to the high-temperature cuprates. This was based on considerations about the electronic properties and on the bilayer structure of the compound formed by edge-sharing, distorted TiO_4Cl_2 octahedra.[3] High-quality single crystals of TiOCl display a kink in the spin susceptibility $\chi(T)$ below about $T_{c2}=92$ K, followed by a pronounced drop at $T_{c1}=67$ K. This leads to a nonmagnetic ground state at T_{c1}, therefore signaling the opening of a singlet-triplet spin gap.[3,4] It has been proposed that the effective dimensionality of the TiO layers is reduced from two to one by an orbital ordering at Ti^{3+} sites and that the singlet ground state is reached by a phase transition also involving lattice degrees of freedom. Consequently, the spin-gap formation and the associated fluctuations in TiOCl emerge in an entirely new perspective from a quantum antiferromagnet, and a scenario based on a spin-Peierls (SP) transition occurring below T_{c1} has been credited as being the most plausible interpretation of the experimental findings.[3]

The title compound seems also to be an ideal material to investigate a broken symmetry ground state with orbital degrees of freedom but without charge ordering. The relevant role played by large electronic energy scales, associated with the orbital degrees of freedom, differentiates TiOCl from $CuGeO_3$ and NaV_2O_5, two other intensively studied spin-Peierls systems. $CuGeO_3$ is characterized by a state without an orbital and charge degrees of freedom, while NaV_2O_5 is characterized by a state with an orbital and charge degrees of freedom.[4–7] In this context, it is worth mentioning that the coupling of an orbital to spin degrees of freedom in a chain system may establish a novel route to the formation of spin-gap states and spin-orbital excitations.[8–10]

Optical methods, such as infrared or Raman spectroscopy, are powerful experimental tools in revealing the characteristic energy scales associated with the development of broken symmetry ground states, driven by magnetic and/or structural phase transitions. Indeed, information on the nature of the electronic (magnetic) ground state, lattice distortion, and interplay of electronic (magnetic) and lattice degrees of freedom can be obtained studying in detail the electronic (magnetic) excitations and the phonon spectrum, as a function of temperature. Furthermore, the role played by strong quantum fluctuations in $S=\frac{1}{2}$ systems, an issue of key importance, can be addressed as well. We provide here a complete set of infrared optical data on TiOCl and a thorough analysis of its electrodynamic response. The paper is organized as follows: we first briefly describe the experiment and present the data;

the discussion will then emphasize the temperature dependence of the phonon spectrum from where we extract relevant information about the spin-gap ground state below T_{c1}.

II. EXPERIMENT AND RESULTS

Our TiOCl single crystals were synthesized by standard vapor-transport techniques from TiO_2 and $TiCl_3$, according to the procedure described in Ref. 11. The crystals were checked by x-ray-diffraction experiments and static magnetic susceptibility.[3,4] TiOCl is an oxyhalogenide with a layered structure made up of $Ti^{3+}O^{2-}$ bilayers separated by Cl^- bilayers. The basic TiO_4Cl_2 octahedra build an edge-shared network in the *ab* plane of the orthorhombic unit cell. $\chi(T)$, besides the already-mentioned kink and sharp drop at T_{c2} and T_{c1}, respectively, is also characterized by a broad maximum around 400 K. Above 100 K, $\chi(T)$ can be fitted by an $S=\frac{1}{2}$ Heisenberg spin-chain model with an antiferromagnetic (AF) exchange coupling constant $J=660$ K (Ref. 3). Furthermore, the specific heat $C_p(T)$ displays an anomaly only at T_{c2} (Ref. 12).

We have measured the optical reflectivity $R(\omega)$ from the far infrared (FIR) up to the ultraviolet (UV) spectral range at temperatures between 10 and 300 K and also as a function of magnetic field. Since we did not find any magnetic-field dependence, we will focus on the temperature dependence only. The Kramers-Kronig (KK) transformation of $R(\omega)$ allows us to evaluate the optical functions, such as the real part $\sigma_1(\omega)$ of the optical conductivity. To this end, $R(\omega)$ was extrapolated to a constant value towards zero frequency (because of the insulating nature of TiOCl) and with ω^{-s} $(2<s<4)$ above 10^5 cm^{-1}. Besides some scattering in the data below 50 cm^{-1}, these extrapolations do not affect or alter the overall shape of the optical properties (see below). Further details pertaining to the experimental method can be found elsewhere.[13] Light was linearly polarized along the chain *b* axis and the transverse *a* axis.[1,3] In order to avoid leakage effects of the polarizer, the polarization of light in our experiment always coincides with the vertical axis of the sample mounting so that the investigated crystallographic direction was perfectly parallel to the polarization of the light beam. Therefore, the polarization dependence was obtained by rotating the sample (instead of the polarizer) by 90° inside the cryostat. This assures that no undesired projections of the light polarization along any transverse crystallographic direction occur in our experiment.

Figure 1 summarizes our results by focusing attention on the temperature dependence of $R(\omega)$ in the infrared spectral range and for both polarization directions. The insets display the whole $R(\omega)$ spectra at 300 K with a logarithmic energy scale. The first obvious observation is the strong anisotropy of the optical response within the *ab* plane and for photon energies below $\sim 10^4$ cm^{-1}. Despite the two-dimensional layeredlike structure, the anisotropy in the infrared spectra may be considered as a signature for the low dimensionality of TiOCl. Figure 2 reproduces the real part $\sigma_1(\omega)$ of the optical conductivity at 300 K in the far-infrared spectral range, as obtained from the KK transformation of $R(\omega)$. We

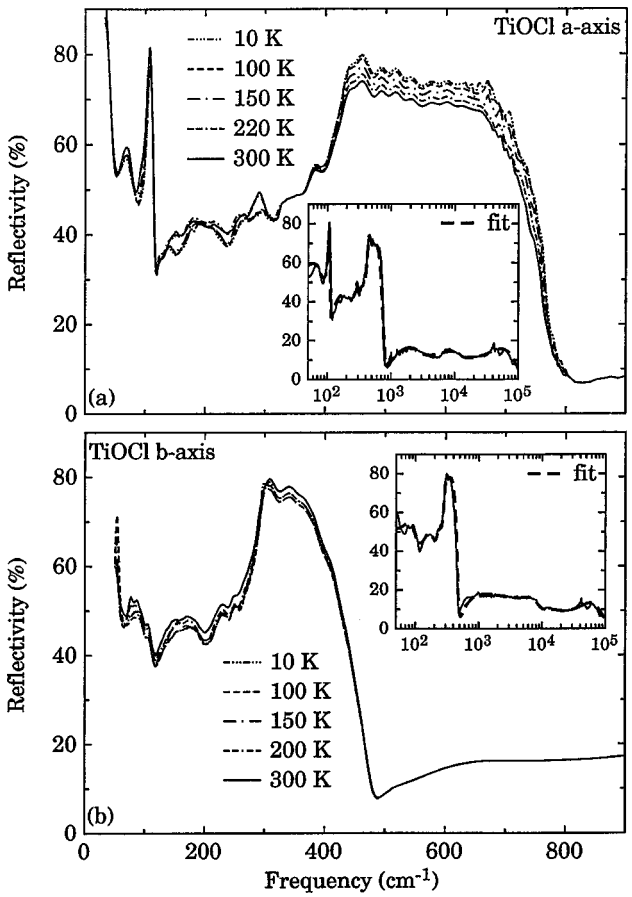

FIG. 1. Optical reflectivity $R(\omega)$ in the infrared spectral range of TiOCl along the *a* axis (a) and *b* axis (b). The insets show the whole spectra at 300 K up to the ultraviolet spectral range and the fit as described in the text.

caution that the features in $\sigma_1(\omega)$ below 50 cm^{-1} for both polarization directions are spurious effects induced by the KK transformations. These features turn out to be temperature-independent and are not considered further in our analysis. The inset in panel (b) enhances the visible spectral range, stressing the feature around 8×10^3 cm^{-1} ($\sim$1 eV) for both polarization directions. Above 4×10^4 cm^{-1}, the $\sigma_1(\omega)$ spectra (not shown here, see Ref. 14 for more details) were found to be polarization-independent.

III. DISCUSSION

The high-frequency part of the excitation spectrum[14] is dominated by electronic interband transitions [Fig. 1 and the inset of Fig. 2(b)]. Recent local density approximation LDA+U calculations,[3] using the linear combination of muffin tin orbitals (LMTO) method, predict a split-off of the (one-dimensional) t_{2g} bands creating an insulating state with a (charge) gap of about 8100 cm^{-1} (1 eV). The t_{2g} band is derived from the d_{xy} orbitals corresponding to the linear Ti chains (i.e., to the orbital ordering at Ti^{3+} sites) along the crystallographic *b* axis,[3] inducing an effective dimensionality reduction from two to one. This agrees with our data displaying a peak at $\sim 8\times10^3$ cm^{-1} along the chain *b* axis and a

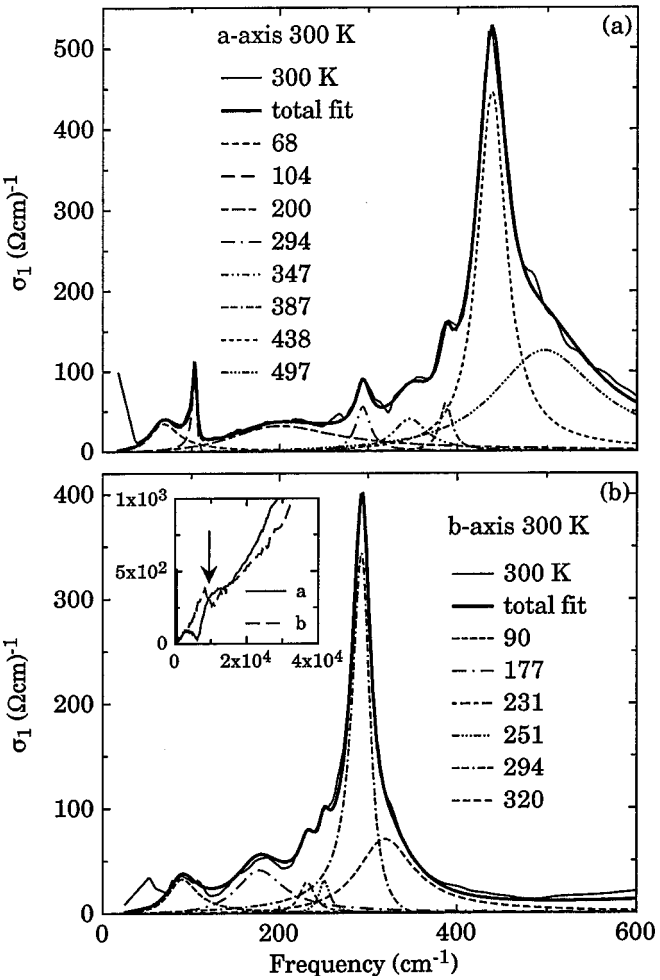

FIG. 2. Real part $\sigma_1(\omega)$ of the optical conductivity at 300 K in the infrared spectral range of TiOCl along the *a* axis (a) and *b* axis (b). The total fit and its components, identified in the legend by their respective resonance frequency in cm^{-1}, are also shown (Ref. 26). The inset enlarges the visible spectral range and the arrow indicates the feature at 8100 cm^{-1} (1 eV) for both polarizations (see text). The temperature dependence of $\sigma_1(\omega)$ was already shown in Ref. 14.

pronounced shoulder at the same energy along the transverse *a* axis [see the arrow in the inset of Fig. 2(b)]. The same band-structure calculations[3] suggest furthermore interband transitions between the O and Cl *p* levels and the Ti *d* levels at energies between 3.2×10^4 and 5.6×10^4 cm^{-1} (4 and 7 eV). This is again very much in agreement with the absorption features seen in our $\sigma_1(\omega)$ spectra (see the insets of Fig. 1 in Ref. 14) along both polarization directions.

In the far-infrared spectral range (main panels of Fig. 1), several absorptions dominate the $R(\omega)$ spectra. The absorption features are better seen in the real part $\sigma_1(\omega)$ of the optical conductivity (Fig. 2). Along the chain *b* axis [Fig. 2(b)], there is a strong peak at 294 cm^{-1} with additional absorptions, overlapped to its low-frequency tail, at 251 and 231 cm^{-1}. Moreover, we recognize broad absorptions at 177 cm^{-1} and around 90 cm^{-1}. Along the transverse *a* axis [Fig. 2(a)], there is a strong peak at 438 cm^{-1} and less intensive absorptions at 68, 104, 294, 347, and 387 cm^{-1}, as

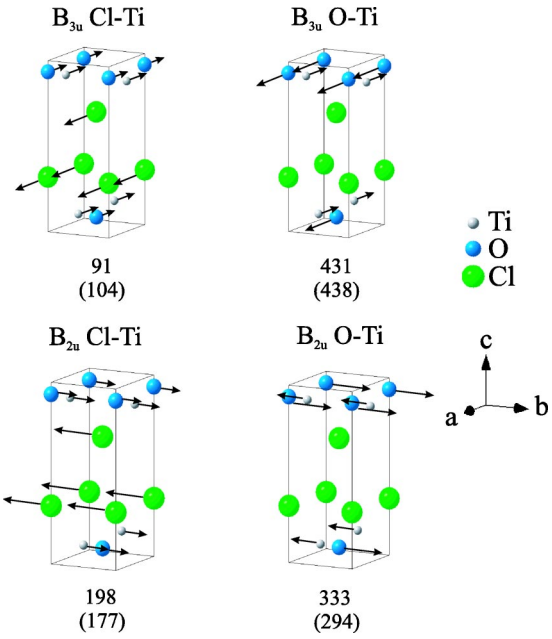

FIG. 3. (Color online) Schematic representation of the eigenvectors for the B_{3u} and B_{2u} normal modes in TiOCl. The atom displacements for the IR-active phonons occur within the *ab* plane. The calculated normal frequencies in cm^{-1} are compared with the observed values (in parentheses).

well as a very broad feature around 200 cm^{-1}. A few absorptions are furthermore characterized by an asymmetric shape (see below). The strongest modes at 294 and 438 cm^{-1} along the *b* and *a* axis, respectively, display rather broad high-frequency tails, which might be indicative of some anharmonicity.

For TiOCl with the bisandwich layer structure of FeOCl-type,[1] the space group $Pmmn(59,D_{2h})$ can be considered at room temperature, for which two B_{3u} modes polarized along the *a* axis, two B_{2u} along the *b* axis, and two B_{1u} along the *c* axis can be predicted as infrared (IR)-active phonons. Because our samples are rather thin, we only have access to the B_{2u} and B_{3u} modes of the *ab* plane. We note that $3A_g$, $3B_{2g}$, and $3B_{3g}$ Raman-active phonons are expected, as well. For light polarized within the *ab* plane, only the $3A_g$ modes, inducing displacements along the *c* axis, can be detected.[14] Classical shell-model calculations allow us to extract eigenfrequencies and eigenvectors for both Raman- and IR-active phonons of TiOCl (Ref. 15). As far as the IR phonons are concerned, the calculations predict the B_{3u} (*a* axis) phonons at 91 and 431 cm^{-1} and the B_{2u} (*b* axis) at 198 and 333 cm^{-1}. The agreement between the calculated frequencies of the fundamental IR phonons and the experimental observation is pretty good. Particularly, the two high-frequency ones can be identified with the most pronounced features in the experimental *a*- and *b*-axis spectra, respectively. Figure 3 shows the normal mode eigenvector patterns for the IR-active phonons, resulting from our shell-model calculations. Table I summarizes the predicted and the so far experimentally determined phonon frequencies for the IR-active modes and, as a complement, for the Raman-active modes[14] as well.

TABLE I. Infrared and Raman active phonons for TiOCl after the space group $P_{mmn}(59,D_{2h})$. The calculated [shell model (Ref. 15)] mode frequencies in cm^{-1} are compared to the experimentally obtained values (in parentheses). A_g modes are observable in (*aa*) or (*bb*) polarization. B_{2g} and B_{3g} modes are only accessible in (*ac*) and (*bc*) polarization, respectively, with one polarization vector parallel to the *c* axis.

Infrared			Raman		
B_{1u}	B_{2u} [a]	B_{3u} [a]	A_g [b]	B_{2g}	B_{3g}
308	198	91	248	84	126
	(177)	(104)	(203)		
433	333	431	333	219	237
	(294)	(438)	(365)		
			431	491	390
			(430)		

[a]This work.
[b]Reference 14.

Even though the calculated frequencies of the IR phonon modes agree well with some features in our spectra, a larger number of phononlike absorptions than theoretically predicted is found for both polarizations. These results on TiOCl are reinforced by our recent optical investigation of the parent TiOBr compound.[16] For both polarization directions, we find the same set of IR-active phonon modes, just shifted in frequency. Particularly, those modes involving the Br ion are normalized (i.e., redshifted) in frequency by the reduced mass with respect to the corresponding modes for the Cl compound.[16] Furthermore, we remark that more phonon modes than expected from the nominal space group have been also detected in other related TiX_2 (X=I, Br, and Cl) compounds.[17]

The sample mounting chosen in our experiment (see above) allows us to exclude leakage effects due to the polarizer. However, one might invoke some twinning of the specimens. This could lead to additional phonon modes, due to the mixing of different polarization directions. This possibility is, nevertheless, rather unlikely because of the strong anisotropy of the optical spectra. If domains would be present because of twinning, phonons for both crystallographic axes would be detected for both polarizations of light and no anisotropy would be found. For instance, the peaks at 387 and 438 cm^{-1} along the *a* axis [Fig. 2(a)] are totally absent in the spectra along the *b* axis [Fig. 2(b)]. The same applies for the sharp feature at about 104 cm^{-1} for the *a* axis. Moreover, as will be discussed in detail below, the temperature dependence in $\sigma_1(\omega)$ can differ substantially even for absorptions coinciding at the same frequency in both polarizations. Therefore, we are confident that no common features are shared in FIR among the two polarizations. One proposal could be that the effective space group corresponds to a lower symmetry than assumed so far.[1] A lower crystal symmetry would then be the consequence of a superstructure, induced, for instance, by orbital ordering. The presence of those additional IR-active modes at 300 K would indicate that the crystal structure of TiOCl is already transformed well above T_{c2}. Thorough x-ray analysis, presently in progress on TiOX, is necessary in order to clarify this issue. Additional modes due to a coupling between the lattice dynamics and the spin system or due to surface inhomogeneity may also become IR-active. Nevertheless, the latter possibility, implying specimen dependence, is rather unlikely, because of the similarity, pointed out above, in the phonon spectrum of the TiOX and TiX_2 series.

In order to shed light on the temperature dependence of the phonon spectrum, we have fitted the optical conductivity with the so-called Fano expression,[18,19]

$$\tilde{\sigma}(\omega)=\sum_j i\sigma_{0j}\frac{(q_j+i)^2}{i+x(\omega)}, \tag{1}$$

with $x(\omega)=(\omega_{0j}^2-\omega^2)/\gamma_j\omega$, where ω_{0j} is the resonance frequency, γ_j is the width (i.e., damping), and $\sigma_{0j}=\omega_{pj}^2/\gamma_j q_j^2$ with ω_{pj} as the oscillator strength and q_j as the so-called asymmetry factor of the j absorption. The asymmetric line shape for the (sharp) phonon modes derives from an interaction between lattice vibrations and a continuum, usually given by an electronic background. The interaction with a magnetic continuum may also lead to a Fano line shape, as shown in the Raman-scattering spectra of low-dimensional spin systems.[7,20] It is verified easily that for the dimensionless Fano parameter $q_j\to\infty$, one can recover the line shape of the harmonic Lorentzian oscillator.[13,18] The approach of Eq. (1) was successfully applied by Damascelli *et al.*[21,22] to the spin-Peierls system α'-NaV_2O_5.

Alternative approaches, based on the Fano theory,[19] are available in the literature. Here, we quote first of all the work by Lupi *et al.*[23] on the phonon interaction with a polaronic background in $Nd_{1.96}Ce_{0.04}CuO_{4+y}$. This approach is based on the extension of Fano's formalism by Davis and Feldkamp (DF),[24] who considered the case of an interaction between an arbitrary number of discrete states and continua. In this work, we will primarily focus our attention on the fits of $\sigma_1(\omega)$ after Eq. (1). Nevertheless, in order to stress the equivalence among different approaches, we will discuss and compare the relevant asymmetry q_j factors obtained with Eq. (1) and by the DF formalism. Secondly, we also mention the discussion of the *c*-axis phonon modes in $YBa_2Cu_3O_y$ by Schützmann *et al.*[25] In this phenomenological approach, the conventional Lorentz shape was modified by a factor $e^{i\theta}$, where θ accounts for the asymmetry. This model, however, does not add relevant physical insight to the discussion with respect to the more simple Lorentz model.[13] Therefore, it will not be considered further.

The total fit of $\sigma_1(\omega)=\mathrm{Re}(\tilde{\sigma}(\omega))$, covering the whole spectral range from FIR up to UV, is obtained by summing over eleven and ten contributions in Eq. (1) for the *a* and *b* axis (Ref. 26), respectively. The fit of $\sigma_1(\omega)$ at 300 K and the single components in FIR for both polarization directions are shown in Fig. 2. The reproduction of the experimental $\sigma_1(\omega)$ curve is astonishingly good and the same fit quality is obtained at all temperatures. In passing, we also note that the same set of fit parameters[26] allows us to reproduce the measured $R(\omega)$ spectra [see, e.g., the fit of $R(\omega)$ at 300 K in the insets of Fig. 1].

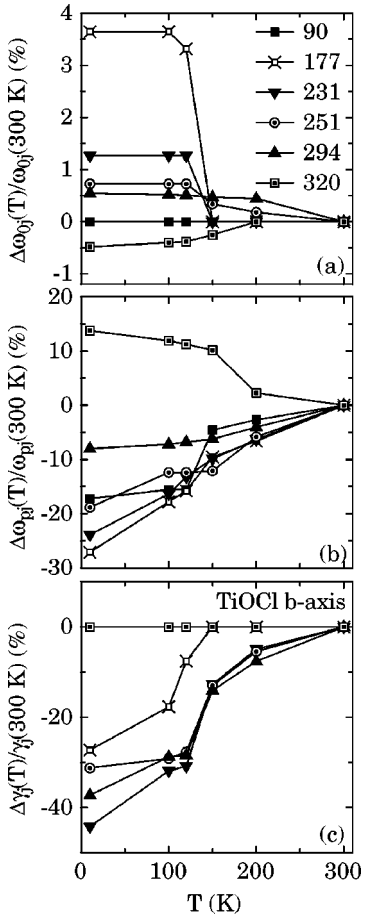

FIG. 4. Temperature dependence along the *b* axis of the percentage change with respect to 300 K (see text) for the resonance frequencies (ω_{0j}) (a), the oscillator strengths (ω_{pj}) (b), and the dampings (γ_j) (c) of the phonon modes (identified in the legend by their respective resonance frequency in cm^{-1}).

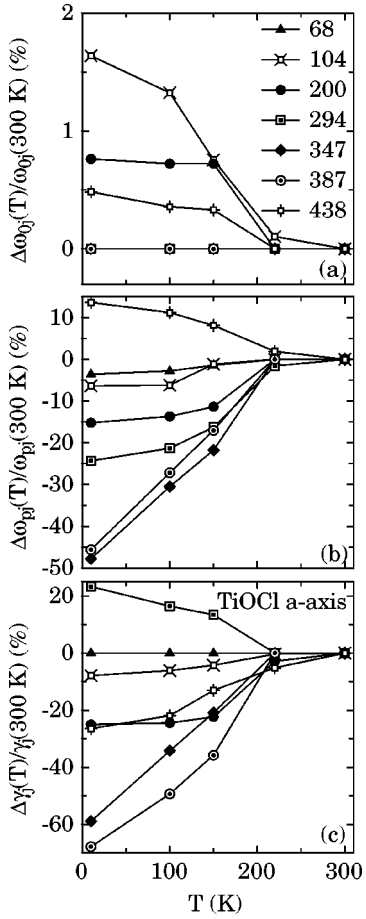

FIG. 5. Temperature dependence along the *a* axis of the percentage change with respect to 300 K (see text) for the resonance frequencies (ω_{0j}) (a), the oscillator strengths (ω_{pj}) (b), and the dampings (γ_j) (c) of the phonon modes (identified in the legend by their respective resonance frequency in cm^{-1}).

The temperature dependence of the fit parameters ($\omega_{0j}, \gamma_j, \omega_{pj}$, and q_j) (Ref. 26) is shown, as a percentage change with respect to the 300-K data [e.g., $\Delta\omega_{0j}(T)/\omega_{0j}(300\ \mathrm{K})$ with $\Delta\omega_{0j}(T)=\omega_{0j}(T)-\omega_{0j}(300\ \mathrm{K})$], in Figs. 4, 5, and 6 for both polarizations. Along the *a* axis, the lower seven oscillators are temperature-dependent, while along the *b* axis the lower six are temperature-dependent, and these will be discussed further here. The overall temperature dependence mainly develops below 200 K and tends to saturate below 100 K (particularly for the chain *b* axis). The temperature dependence, occurring in a broad temperature interval and extending well above T_{c1}, is indicative of an extended fluctuation regime, which has been recognized in NMR data,[4] as well. The relaxation rates of ^{35}Cl sites show dynamic lattice distortion with onset at 200 K, while for the ^{46,49}Ti sites, $1/TT_1$, which probes the spin degrees of freedom, forms a maximum at about 135 K (Ref. 4). Therefore, the interplay between the lattice and spin degrees of freedom must be already taking place at high temperatures. The temperature dependence of $1/TT_1$ implies a pseudogap phase in the homogeneous state of the spin system with an estimated pseudogap $\Delta_{\mathrm{fluct}}\sim 430$ K (Ref. 4). The temperature dependence of the electron-spin-resonance (ESR) parameters (i.e., the ESR linewidth ΔH and the so-called ESR *g* tensor) also displays a progressive evolution over a broad temperature range between 200 K and T_{c1} (Ref. 27). From the analysis of the ESR signal, it is claimed that a strong coupling between spin and lattice degrees of freedom exists and that spin as well as orbital fluctuation effects above T_{c1} may be responsible for the peculiar temperature dependence of various quantities [e.g., $\chi(T)$].

The resonance frequencies (ω_{0j}) of almost all phonons tend to increase [Figs. 4(a) and 5(a)], though moderately (i.e., the change does not exceed 4%), with decreasing temperature, indicating a progressive hardening of the modes. The resonance at 320 cm^{-1} along the *b* axis, accounting for the broad high-frequency tail of the mode at 294 cm^{-1}, displays on the contrary a weak softening. A well-defined soft mode is in principle expected in models for the conventional SP transition where the structural deformation is driven by a linear coupling between the lattice and the magnetic degrees of freedom. As far as the dynamical interplay between spins and phonons in TiOCl is concerned, it is clear from the temperature dependence of our optical spectra that neither a soft mode nor a generalized redshift in the resonance frequency of the phonons has been detected. At this point, apart from

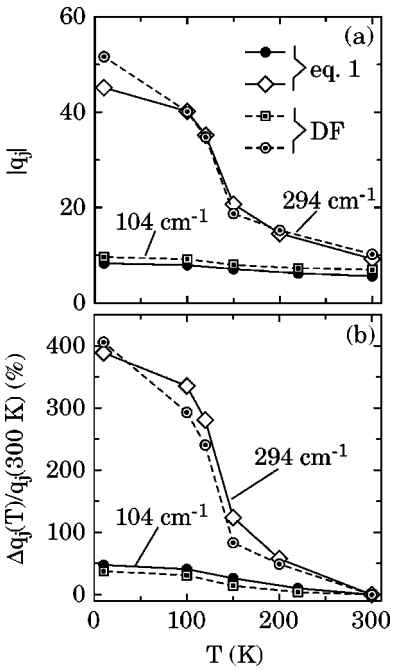

FIG. 6. (a) Temperature dependence of the asymmetry factor $|q_j|$ for the 104-cm^{-1} mode along the *a* axis and the 294-cm^{-1} mode along the *b* axis, calculated after Eq. (1). Note that $q_j<0$ for both polarization directions. (b) Temperature dependence of the corresponding percentage changes with respect to 300 K [i.e., $\Delta q_j(T)/q_j(300\ \mathrm{K})$, with $\Delta q_j(T)=q_j(T)-q_j(300\ \mathrm{K})$] for the asymmetry factor q_j of the *a* and *b* axes. In addition, we also display the q_j factor and its percentage change for both modes obtained with the Fano formalism, based on the approach of Davis and Feldkamp (DF) (Ref. 24). The equivalence of the two approaches [Eq. (1) and DF] is obvious.

the 320-cm^{-1} mode along the *b* axis, it seems that the transition at T_{c1} is not driven by a softening of the IR phonon spectrum. A final word on the soft mode issue will only be possible with neutron-scattering experiments, since the lattice dimerization involved in the Peierls transition is related to normal modes away from the Brillouin-zone center. From the perspective of the IR spectrum, one could have hoped that the presence of a soft mode would have resulted in an overall softening of the phonon branch to which it belongs. The absence of a clear signature for IR phonon softening is common to other spin-Peierls systems, such as $CuGeO_3$ (Ref. 28). Nevertheless, evidence for phonon softening has been found in the Raman scattering experiments.[14] A broad feature was identified at about 160 cm^{-1} for the chain *b*-axis polarization. The weight of this signal gets confined and softens down to 130 cm^{-1}, i.e., by $\sim$20%, with decreasing temperature. This mode is ascribed to a Brillouin-zone boundary phonon. The experimentally observed A_g mode at 203 cm^{-1} (Table I) with light polarization along the *b* axis is its related Γ-point Raman-allowed phonon.[14]

Most of the phonon modes get narrow with decreasing temperature [Figs. 4(c) and 5(c)]. Only the mode at 294 cm^{-1} along the *a* axis displays a broadening with decreasing temperature. Particularly the width γ_j of all phonons along the chain *b* axis follows very closely the temperature dependence of the magnetic susceptibility $\chi(T)$. The temperature dependence of γ_j in TiOCl is very similar to the findings in α'-NaV_2O_5 (Ref. 21). The pronounced narrowing of the modes occurs in the temperature interval of the so-called pseudo-spin-gap phase identified in the NMR spectra.[4] It seems, therefore, natural to relate this phonon narrowing to the suppression of low-frequency spin fluctuations and to consider it as another fingerprint for the coupled spin-lattice fluctuations.[14]

It turns out that most of the absorptions, seen in our spectra (Figs. 1 and 2) and described by the *j* components in Eq. (1), reduce to the Lorentzian-like (i.e., $q_j\rightarrow\infty$) shape. Only the peak at 104 cm^{-1} along the *a* axis and the peak at 294 cm^{-1} along the *b* axis display a Fano-like asymmetry. The asymmetry (Fig. 6) of the mode at 104 cm^{-1} along the *a* axis gradually decreases (i.e., $|q_j|$ gets larger) with decreasing temperature, although the mode remains considerably asymmetric at all temperatures. This indicates that there is a predominant interaction with the continuum both above and below T_{c1}. On the other hand, the temperature dependence of the asymmetry for the 294-cm^{-1} mode along the *b* axis displays a clear crossover between 200 K and T_{c2} from an asymmetric Fano-like shape (i.e., $|q_j|$ small) to a Lorentzian oscillator (i.e., $|q_j|$ very large). The distinct behavior in the temperature dependence of the q_j factors within the *ab* plane is a further fingerprint for the anisotropy of the lattice dynamics as well as of the coupling between phonon and continuum, and could hint at a low dimensionality of TiOCl. The clear Fano-Lorentz crossover along the chain *b* axis suggests, moreover, the suppression of the interaction with the continuum with decreasing temperature.[21] Since $q_j<0$ for both asymmetric modes, the relevant continuum of excitations, which is renormalized with temperature, covers an energy interval below the phonon resonance frequencies. For the chain *b* axis, this identifies a characteristic energy scale of the order of 400 K (see below the discussion of the spectral weight redistribution). In Fig. 6, we also report, for comparison, the q_j factor for both modes as calculated from the Fano model based on the approach of Davis and Feldkamp.[24] Even though the two Fano approaches[18,24] [Eq. (1) and DF] are formally different (i.e., they are characterized by different energy power-law decays of the absorption coefficient), the corresponding q_j factors are identical both in absolute value[26] and in the relative percentage change (Fig. 6). This stresses the equivalence of the Fano asymmetry concept (parametrized by the q_j factors) for both calculations.

The temperature dependence of the spectral weight encountered in the phonon spectrum is also of interest. We have observed[14] that the spectral weight encountered in $\sigma_1(\omega)$ at low frequencies tends to decrease below 200 K. The total spectral weight, obtained by integrating $\sigma_1(\omega)$ up to the UV spectral range, however, is conserved and it is fully recovered already by 10^4 cm^{-1} ($\sim$1 eV).[14] This is confirmed by the behavior of the squared (ω_{pj}^2) oscillator strengths [Figs. 4(b) and 5(b)]. Particularly for the *b* axis, the spectral weight is progressively removed with decreasing temperature over a spectral range of roughly 400 K. This is in agreement with the energy scale identified above in the analysis of the phonon asymmetry within the Fano approach. Most of the sup-

pressed weight at low frequencies moves into the modes at 294 or 438 cm^{-1} or into their high-frequency tails along the *b* and *a* axes, respectively. The remaining part of the suppressed weight shifts from the elastic degrees of freedom toward zone-boundary (folded) modes or, as we favor for TiOCl, to the electronic degrees of freedom at high energies. Again, this overall shift mainly occurs between T_{c2} and 200 K.

Finally, the giant reduction of the phonon width, the behavior of the Fano q_j factors (particularly along the *b* axis), as well as the suppression of spectral weight in FIR (Figs. 4, 5, and 6) suggest the presence and development of a characteristic energy scale. Above all, the depletion of spectral weight over an energy range of the order of 400 K is very much reminiscent of a similar behavior in the Raman spectra, occurring over the same energy interval with decreasing temperature and associated with the spin-gap opening.[14] Setting $2\Delta_{opt} \sim 300$ cm^{-1} (~ 430 K) as the lower bound for the spin-gap energy, we obtain a reduced gap ratio $2\Delta_{opt}/k_B T_{c1} \sim 4.6$ and 6.7 for T_{c2} and T_{c1}, respectively. With respect to the mean-field results (i.e., $2\Delta/k_B T_c \sim 3.52$), our larger gap ratios might reveal competing exchange paths or electronic degrees of freedom,[14] but they are more reasonable than those obtained from recent NMR study.[4] Indeed, the extraordinary larger spin gap Δ_{fluct} would correspond to a reduced gap ratio ranging between 9 and 13 for T_{c1} and T_{c2}, respectively. One can reconcile the outcome of a typical local probe such as NMR with the optical results, which notably give an average perspective of the excitation spectrum, by following the development of both the magnetic and structural correlations. With decreasing temperature down to T_{c2}, the coherence length of the structural distortion increases and the magnetic correlations crossover from 2D to 1D (Ref. 14). The energy gain at $T < T_{c2}$ is mainly related to the spin system. Therefore, the related anomaly in the specific heat[12] is small, and in conventional x-ray scattering no sign of a coherent structural distortion can be found.[27] With further decreasing *T*, the structural distortion becomes long-range. Below T_{c1}, TiOCl has a conventional behavior closely related to a spin-Peierls system. Therefore, the spin gap $2\Delta_{fluct}$ [from NMR (Ref. 4)] is the lowest energy for the local double spin flip in the short-range-order distorted phase, while $2\Delta_{opt}$ (from IR and Raman[14]) is the energy for the global spin gap of the fully dimerized chain.

IV. CONCLUSION

We have provided a thorough analysis of the optical properties of TiOCl, emphasizing particularly the temperature dependence of the phonon spectrum. The temperature dependence of all relevant parameters, including the phonon linewidth and the spectral weight, occurs over a broad temperature interval from T_{c1} up to 200 K. This is a fingerprint for the important role played by fluctuation effects. The pronounced narrowing of the IR modes with decreasing temperature coincides with the suppression of low-frequency spin fluctuations, recognized in the spin-gap phase of the NMR spectra.[4] The behavior of the IR spectral weight with temperature establishes the presence of a characteristic energy scale associated with the opening of a spin gap. Although similar findings are frequently observed in 1D systems, the present case is different due to the unusually high energy scale involved.

Summing up, TiOCl, a prototype low-dimensional spin-$\frac{1}{2}$ quantum compound, is a member of a class of correlated electron systems where a pseudogap state is related to large phonon anomalies. Such systems have recently gained importance due to the investigation of so-called orbital liquids[29] and due to the reconsideration of electron-phonon coupling in high-temperature superconductors.[30]

ACKNOWLEDGMENTS

The authors wish to thank J. Müller for technical help, and A. Damascelli, B. Schlein, P. Calvani, and A. Perucchi for fruitful discussions. This work has been supported by the Swiss National Foundation for the Scientific Research, INTAS 01-278, DFG SPP1073 and by the MRSEC Program of the National Science Foundation under award number DMR 02-13282.

[1] R.J. Beynon and J.A. Wilson, J. Phys.: Condens. Matter **5**, 1983 (1993).
[2] A. Seidel and P.A. Lee (private communication).
[3] A. Seidel, C.A. Marianetti, F.C. Chou, G. Ceder, and P.A. Lee, Phys. Rev. B **67**, 020405(R) (2003).
[4] T. Imai and F.C. Chou, e-print cond-mat/0301425.
[5] H. Smolinski, C. Gros, W. Weber, U. Peuchert, G. Roth, M. Weiden, and Ch. Geibel, Phys. Rev. Lett. **80**, 5164 (1998).
[6] M.V. Mostovoy, D.I. Khomskii, and J. Knoester, Phys. Rev. B **65**, 064412 (2002).
[7] P. Lemmens, G. Güntherodt, and C. Gros, Phys. Rep. **375**, 1 (2003).
[8] S.K. Pati, R.R.P. Singh, and D.I. Khomskii, Phys. Rev. Lett. **81**, 5406 (1998).
[9] Y. Yamashita, N. Shibata, and K. Ueda, J. Phys. Soc. Jpn. **69**, 242 (2000).
[10] A.K. Kolezhuk, H.-J. Mikeska, and U. Schollwöck, Phys. Rev. B **63**, 064418 (2001).
[11] H. Schaefer, F. Wartenpfuhl, and E. Weise, Z. Anorg. Allg. Chem. **295**, 268 (1958).
[12] Y.S. Lee, E. Abel, and F.C. Chou (private communication).
[13] F. Wooten, in *Optical Properties of Solids* (Academic Press, New York, 1972), and M. Dressel and G. Grüner, in *Electrodynamics of Solids* (Cambridge University Press, Cambridge, 2002).
[14] P. Lemmens, K.Y. Choi, G. Caimi, L. Degiorgi, N.N. Kovaleva, A. Seidel, and F.C. Chou, cond-mat/0307502 (unpublished).
[15] N.N. Kovaleva (unpublished).
[16] G. Caimi, L. Degiorgi, P. Lemmens, and F.C. Chou (unpublished).
[17] C.H. Maule, J.N. Tothill, P. Strange, and J.A. Wilson, J. Phys.:

Condens. Matter **21**, 2153 (1988).
[18] C. Thomsen, in *Topics in Applied Physics: Light Scattering in Solids VI*, edited by M. Cardona and G. Güntherodt (Springer Verlag, Berlin, 1991), Vol. 68, p. 327.
[19] U. Fano, Phys. Rev. **124**, 1866 (1961).
[20] K.-Y. Choi, G. Güntherodt, A. Oosawa, H. Tanaka, and P. Lemmens, Phys. Rev. B **68**, 174412 (2003).
[21] A. Damascelli, D. van der Marel, M. Grüninger, C. Presura, T.T.M. Palstra, J. Jegoudez, and A. Revcolevschi, Phys. Rev. Lett. **81**, 918 (1998).
[22] A. Damascelli, C. Presura, D. van der Marel, J. Jegoudez, and A. Revcolevschi, Phys. Rev. B **61**, 2535 (2000).
[23] S. Lupi, M. Capizzi, P. Calvani, B. Ruzicka, P. Maselli, P. Dore, and A. Paolone, Phys. Rev. B **57**, 1248 (1998).
[24] L.C. Davis and L.A. Feldkamp, Phys. Rev. B **15**, 2961 (1977).
[25] J. Schützmann, S. Tajima, S. Miyamoto, Y. Sato, and R. Hauff, Phys. Rev. B **52**, 13 665 (1995).
[26] The complete set of fit parameters for all temperatures can be found at the following link: http://www.solidphys.ethz.ch/spectro/suppinfo/TiOCl.pdf
[27] V. Kataev, J. Baier, A. Möller, L. Jongen, G. Meyer, and A. Freimuth, Phys. Rev. B **68**, 140405 (2003).
[28] A. Damascelli, D. van der Marel, F. Parmigiani, G. Dhalenne, and A. Revcolevschi, Phys. Rev. B **56**, R11 373 (1997).
[29] J.v.d. Brink, G. Khaliullin, and D. Khomskii, *Colossal Magnetoresistive Manganites*, edited by T. Chatterji (Kluwer Academic Publishers, Dordrecht, The Netherlands, 2000).
[30] A. Lanzara, P.V. Bogdanov, X.J. Zhou, S.A. Kellar, D.L. Feng, E.D. Lu, T. Yoshida, H. Eisaki, A. Fujimori, K. Kishio, J.-I. Shimoyama, T. Noda, S. Uchida, Z. Hussain, and Z.X. Shen, Nature (London) **412**, 510 (2003).